

Plasmonic hybrid terahertz photomixer of graphene nanoantenna and nanowires

Reiam Al-Mudhafar, Hussein Ali Jawad

Institute of Laser for Postgraduate Studies, University of Baghdad, Baghdad, Iraq

Article Info

Article history:

Received Aug 25, 2021

Revised Dec 19, 2021

Accepted Jan 19, 2022

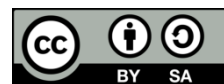
Keywords:

Graphene
Nanoantenna array
Plasmonics
Silver nanowire
Terahertz photomixer

ABSTRACT

Due to their attractive properties, silver nanowires (Ag-NWs) are newly used as nanoelectrodes in continuous wave (CW) THz photomixer. However, since these nanowires have small contact area, the nanowires fill factor in the photomixer active region is low, which leads to reduce the nanowires conductivity. In this work, we proposed to add graphene nanoantenna array as nanoelectrodes to the silver nanowires-based photomixer to improve the conductivity. In addition, the graphene nanoantenna array and the silver nanowires form new hybrid nanoelectrodes for the CW-THz photomixer leading to improve the device conversion efficiency by the plasmonic effect. Two types of graphene nanoantenna array are proposed in two separate photomixer configurations. These are the graphene nanodisk (GND) array and the graphene bow-tie nanoantenna (GNA) array. The photomixer active region is simulated using the computer simulation technology (CST) Studio Suite® for three optical wavelengths: 780 nm, 810 nm, and 850 nm. From the results, we found that the electric field in the active region is enhanced by 4.2 and 4.8 times for the aforementioned configurations, respectively. We also showed that the THz output power can be enhanced by 310 and 530 times, respectively.

This is an open access article under the [CC BY-SA](https://creativecommons.org/licenses/by-sa/4.0/) license.



Corresponding Author:

Reiam Al-Mudhafar
Institute of Laser for Postgraduate Studies, University of Baghdad
Jadriah, P.O box 47314, Baghdad, Iraq
Email: reiam.al-mudhafar@ilps.uobaghdad.edu.iq

1. INTRODUCTION

The utilization of the terahertz (THz) spectrum (between 0.1 and 10 THz) in a wide range of applications like in medical imaging, material science, security, and wireless communications led to increased demands for improving the THz sources [1]–[4]. The main required improvements are in obtaining high THz output power with higher cut-off frequency [5], [6]. The THz Photomixer is a prevalent technique for generating continuous wave (CW) THz frequency due to the wide tunability, low cost, compactness, simplicity, and its room temperature operation [1], [7]–[9].

The conventional technique of designing a photomixer utilizes interdigitated electrodes fabricated on photoconductive material [10], [11]. The photoconductive material with fabricated electrodes forms the active region of the photomixer [10]. The active region is illuminated by the optical beat signal of two CW laser beams. Thereafter, the photogenerated current is modulated with THz frequency (the frequency of the beat signal) and collected by the electrodes [8]. THz waves are then radiated out by a suitable antenna connected to the electrodes [1], [10].

The low efficiency of the optical to THz conversion is the main disadvantage of the conventional photomixer [5], [10]. Many efforts were devoted to improving the conversion efficiency by increasing the light intensity in the photomixer active region. By enhancing the light intensity, the photocurrent will be

increased and hence improving the THz output power [6], [12]–[15]. The THz generated power $P(\omega)$ can be expressed as a function of the light intensity [16]:

$$P(\omega) = \left(\frac{W e \mu_e \tau}{L h f_s} (1 - R)(1 - e^{-\alpha T}) \right)^2 \left(\frac{m R_{ant} V_B^2}{(1 + (\omega_{THz} R_{ant} C)^2)(1 + (\omega_{THz} \tau)^2)} \right) I_0^2 \quad (1)$$

where L is the electrodes length, W is the electrodes width, μ_e is the mobility of the electron, τ is the lifetime of the carriers, f_s is the two laser beams frequency, e is the charge of the electron, h is the Plank constant, R is the reflectivity of the photoconductive material surface, α is the absorption coefficient, R_{ant} is the THz antenna resistance, T is the photoconductive material absorption depth, m is the efficiency of the two laser beams mixing, V_B is the bias voltage, ω_{THz} is the frequency of the beat signal, C is the capacitance of the electrodes, I_0 is the average incident intensity.

The nanostructured configurations and plasmonic structures received much research efforts in recent years. This is mainly because of their roles in increasing the optical absorption and the illumination intensity [17]–[21]. Therefore, they have been intensively used to fabricate THz photomixer electrodes. Yang *et al.* [13] fabricated plasmonic gratings as nanoelectrodes on LTG-GaAs substrate. In his work, the usage of metallic gratings as nanoelectrodes enhances the incident light concentration by the plasmonic effect. In addition, the nanosized dimensions of the electrodes reduce the photocarriers' path lengths. As a result, the obtained THz power was three times higher than the conventional photomixers output power. Ironside *et al.* [6] proposed a metamaterial design structure to enhance the light intensity in the photomixer. In his structure, LTG-GaAs is placed between ultrathin metal-dielectric gratings to obtain a multiplicative enhancement. By improving the optical absorption and decreasing the photocarriers path distance, a THz power in the milliwatt range was obtained. The prime enhancement in the THz photomixer of silver nanowires (Ag-NWs) nanoelectrodes is a consequence of surface plasmon polaritons (SPPs) excitation demonstrated in [22], [23]. Those SPPs waves are excited on the surface of Ag-NWs by near-infrared incident light [22]. While Jumaah *et al.* [24] fabricated a hybrid photomixer by adding nitrogen-doped single-layer graphene nanoflakes to Ag-NWs based photomixer. In his structure, the Ag-NWs conductivity is assumed to be improved by the transportation of the photocarriers via spatial plasmonic field through the dispersed graphene flakes. Additionally, because of the graphene's high thermal conductivity, these nanoflakes promote heat transport in the photomixer. The hybrid photomixer shows a THz output power three times higher than the conventional photomixer output power.

In this work, instead of utilizing dispersed graphene flakes, the graphene nanoantenna bow-tie shape (GNA) and the graphene nanodisk (GND) arrays are proposed in two configurations of photomixer. These arrays are used as nanoelectrodes in addition to Ag-NWs for CW-THz photomixer. These nanoelectrodes can enhance the light intensity in the photomixer. Moreover, the proposed configurations will benefit from the unique properties of graphene to improve the device's electrical and thermal properties.

This article is structured into four sections. The three remaining sections of this paper: section 2 explains the research method and the designs of the active region configurations proposed in this work. Section 3 presents the simulation results with the discussion. Finally, the conclusion and the future work are presented in section 4.

2. RESEARCH METHOD

This section is devoted to describing the method used to evaluate the THz power enhancement of each proposed configuration. Computer simulation technology (CST Studio Suite®) is used to simulate the configurations under investigation. Two simulation approaches are available to investigate the enhancement in the THz output power. The first approach considers evaluating both the active region and the THz antenna performance in a single simulation. The advantage of this approach is that it allows calculating the THz output power directly from the simulation and subsequently estimating the enhancement. This approach, however, requires significant computational time. The second approach considers simulating the active region alone. The result of the electric field is then used to calculate the THz power enhancement by using (1). The main advantage of this approach is that it allows estimating the possible THz power enhancement with a significant reduction in the computational time in comparison to the first approach. Therefore, the latter approach is chosen in our work.

This section is divided into two subsections. The first subsection describes the design of the proposed configurations. It also presents the materials used for each configuration and their dimensions. The simulation setup is then explained in the second subsection.

2.1. The photomixer active region configurations

Two configurations for the active region of the THz photomixer are proposed and simulated in this work. Figures 1 and 2 illustrate the structure of the proposed configurations with their dimensions. A third configuration, which consists of only Ag-NWs nanoelectrodes is also simulated for comparison purposes. The three configurations are described: i) the 1st configuration (reference configuration) has two Ag-NWs nanoelectrodes only, ii) the 2nd configuration has hybrid nanoelectrodes consisting of a GND array and two Ag-NWs, as shown in Figures 1(a) and (b), and iii) the 3rd configuration has hybrid nanoelectrodes consisting of a GNA array and two Ag-NWs, as shown in Figure 2(a)-(c).

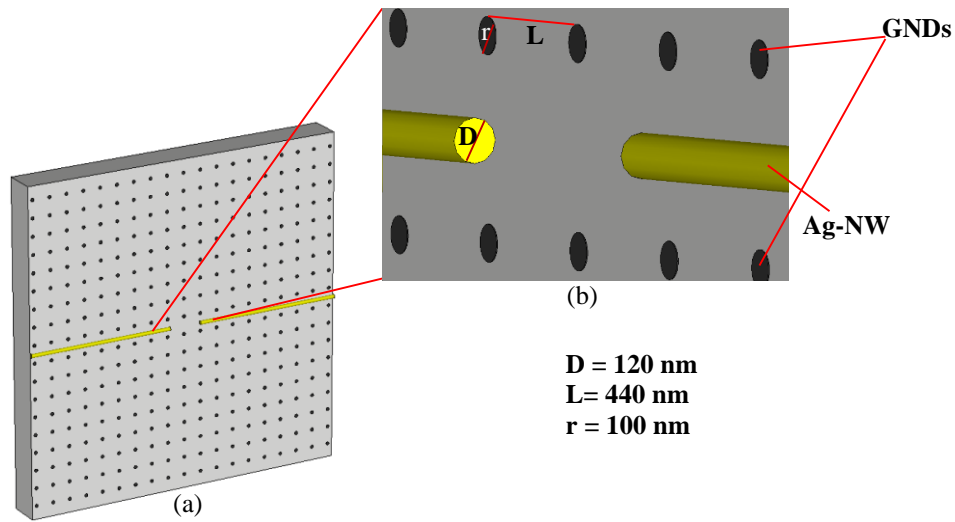


Figure 1. The 2nd configuration (a) the schematic diagram of the configuration and (b) the two Ag-NWs nanoelectrodes gap width of 1 μm

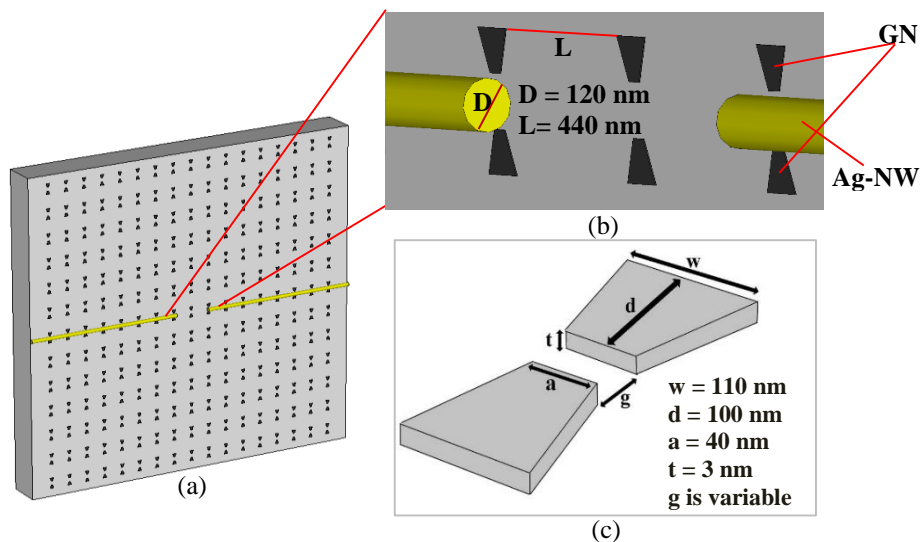


Figure 2. The 3rd configuration (a) the schematic diagram of the configuration, (b) the two Ag-NWs nanoelectrodes gap width of 1 μm , and (c) the schematic diagram of GNA

The nanoelectrodes in all configurations are placed on the GaAs substrate which has a relative permittivity of 12.94. The area of the three configurations is 10 x10 μm^2 and the substrate thickness is 1 μm . The GND array in the second configuration is a two-dimensional periodic array of graphene nanodisk as shown in Figure 1(a). GND has a diameter of 100 nm and a thickness of 3 nm as shown in Figure 1(b). While

the GNA array in the third configuration is a two-dimensional periodic array of graphene bow-tie-shaped nanoantenna as shown in Figure 2(a). To obtain a high field enhancement, the two Ag-NWs nanoelectrodes in the third configuration are positioned in the GNAs' gaps center as shown in Figure 2(b). The bow-tie antenna structure parameters: $w=110$ nm is the antenna width along the x-axis, $d=100$ nm is the length of the antenna arm along the y-axis, $t=3$ nm is the antenna thickness, $a=40$ nm is the width of the antenna tip, and g is the width of the antenna gap as shown in Figure 2(c). The array space in the hybrid configurations is proposed to be 440 nm. In all configurations, Ag-NWs have a diameter and a length of 120 nm and 4.5 μm , respectively. The nanowires' gap width is 1 μm .

2.1. The simulation of the photomixer active region

The two excitation laser beams of the photomixer are modeled as a plane wave circularly polarized with an optical electric field of 1 V/m. In the simulation, three incident optical wavelengths (the common photomixer excitation wavelengths): 780 nm, 810 nm, and 850 nm are applied. The propagation of the incident plane wave is along the z-axis, and thus, the configurations are illuminated from the front side.

The hybrid electrodes in all configurations are in nanosized dimension. Therefore, a high mesh density is required to simulate these configurations. Thus, the performance evaluation of the active region and the THz antenna in a single simulation would consume a long computational time. Therefore, only the photomixer active region is simulated as opposed to simulating the entire structure. The estimated THz power enhancement is then calculated using (1). To achieve a good compromise between the computational time and the simulation accuracy, a mesh resolution of six cells per optical wavelength for the active region is chosen. Additionally, for accurate simulation results, the graphene thickness is divided into three mesh cells by using the local mesh feature. CST allows to create the graphene material and presents it in two models [25], [26]. The first model characterizes the graphene material as a thin metal by surface conductivity. The second model characterizes it with real and imaginary permittivity as a drude-like material [25]–[27]. To characterize graphene in the visible region, only the interband part of graphene conductivity is considered [28]. The graphene conductivity (σ_0) is approximately a constant value across the whole visible region. This value is described by the following equation: ($\sigma_0 = e^2/(4\hbar)$), where e is the charge of the electron and \hbar is the reduced Planck constant). This approximate value of the graphene conductivity can also be used to determine the graphene permittivity [28], [29]. Graphene parameters of zero chemical potential, 0.1 ps relaxation time at 293 K temperature are defined in the simulation.

The time-domain solver of electromagnetic (EM) numerical simulation is used to calculate the distribution of EM field in the photomixer active region. The electric field variation in the three configurations is studied as a function of the incident wavelengths. In the third configuration, the electric field variation is studied at different GNA gap widths (124 nm, 130 nm, 134 nm, 140 nm, and 144 nm). All the other design parameters are kept the same. The thickness of the GND and the GNA is kept unchanged at 3 nm, which is equivalent to the thickness of nine graphene layers [30]. Thereafter, the GND and GNA thicknesses are varied with 2.4 nm, 3 nm, and 3.7 nm, which are equivalent to thicknesses of 7, 9, and 11 layers of graphene, respectively. Finally, the electric field is examined for each of those thicknesses.

3. RESULTS AND DISCUSSION

The simulation aims to evaluate the electric field distributions in all three configurations for the three incident wavelengths presented earlier. By doing so, we will be able to validate if our assumptions of introducing GND and GNA to the Ag-NWs based photomixer will indeed enhance the electric field inside the structure. Figure 3 is devoted to show the simulation results of the maximum electric field in all configurations for the three wavelengths.

We can observe from the results that the two hybrid configurations indeed introduce a significant enhancement in the maximum electric field in comparison to the first configuration. In addition, this enhancement is observed over all three incident wavelengths. The highest field enhancement is obtained at 850 nm incident wavelength. While the incident signal at 810 nm exhibits the smallest enhancement in both of the hybrid configurations. The maximum electric field in the second configuration is (3.4, 1.8, and 3.8) times higher than the field in the first one for 780 nm, 810 nm, and 850 nm wavelengths, respectively. The same figure also shows the maximum electric field in the third configuration for five different GNA gap widths. In there, the maximum electric field shows its highest value, when the smallest gap width of 124 nm is selected. At this gap width, the maximum electric field is (3.7, 2.1, and 4.4) times higher than the field in the first configuration for the aforementioned wavelengths, respectively. Consequently, the third configuration with the smallest GNA gap width exhibits the highest field enhancement in comparison to the other two configurations.

Since the highest enhancement is achieved at 850 nm incident wavelength, we choose this wavelength to analyze and discuss the electric field distributions in all three configurations. Figure 4

illustrates the distributions of the electric field z-component at this wavelength in all configurations. From Figures 4(a)-(c), one can see a very high electric field on the Ag-NWs surfaces and around the area adjacent to them for first, second, and third configurations, respectively. This high field is a consequence of SPPs excitation on the nanowires` surfaces by near-infrared incident light [22], [23].

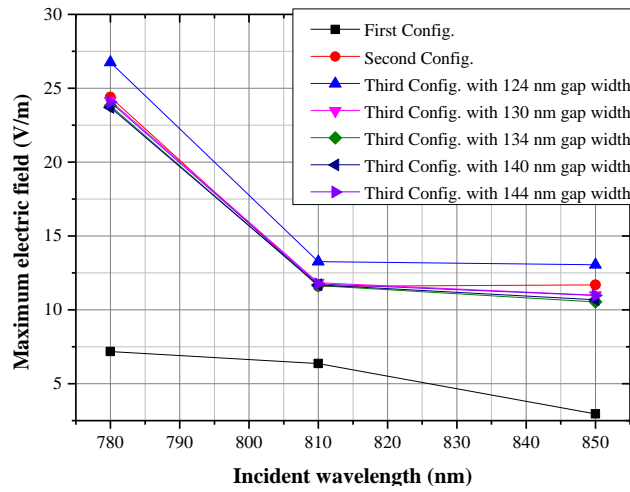


Figure 3. The maximum electric field as a function of the incident wavelengths for the three configurations

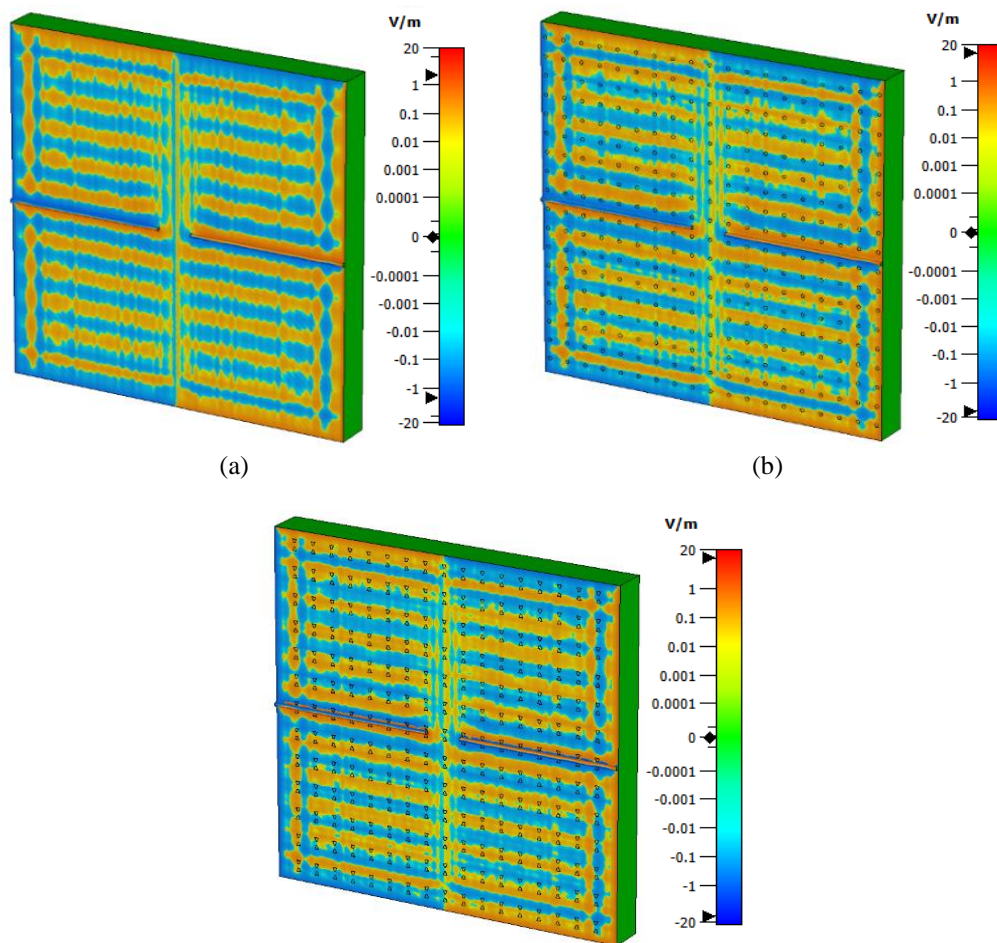


Figure 4. Distributions of the electric field z-component at 850 nm incident wavelength: (a) the 1st configuration, (b) the 2nd configuration, and (c) the 3rd configuration with GNA gap width of 124 nm

To further analyze the field distributions in these regions for all configurations in detail, we present Figures 5 and 6. The x- and the y-axis, presented in the labels of the two figures, are the axes whose origin is at the center of the structure. From Figures 5(a)-(c), we can see that the electric field on the Ag-NWs surfaces is enhanced by the incident light confinement introduced by adding GND and GNA to the active region [24], [31]. The confinement of the incident light by GNDs and GNAs located near Ag-NWs leads to enhance the light field intensity in this region. As a result, the enhanced light in the Ag-NWs neighboring area improves the plasmonic field on their surfaces. Therefore, the second and the third configurations exhibit a significant enhancement in the electric field on the nanowire surfaces.

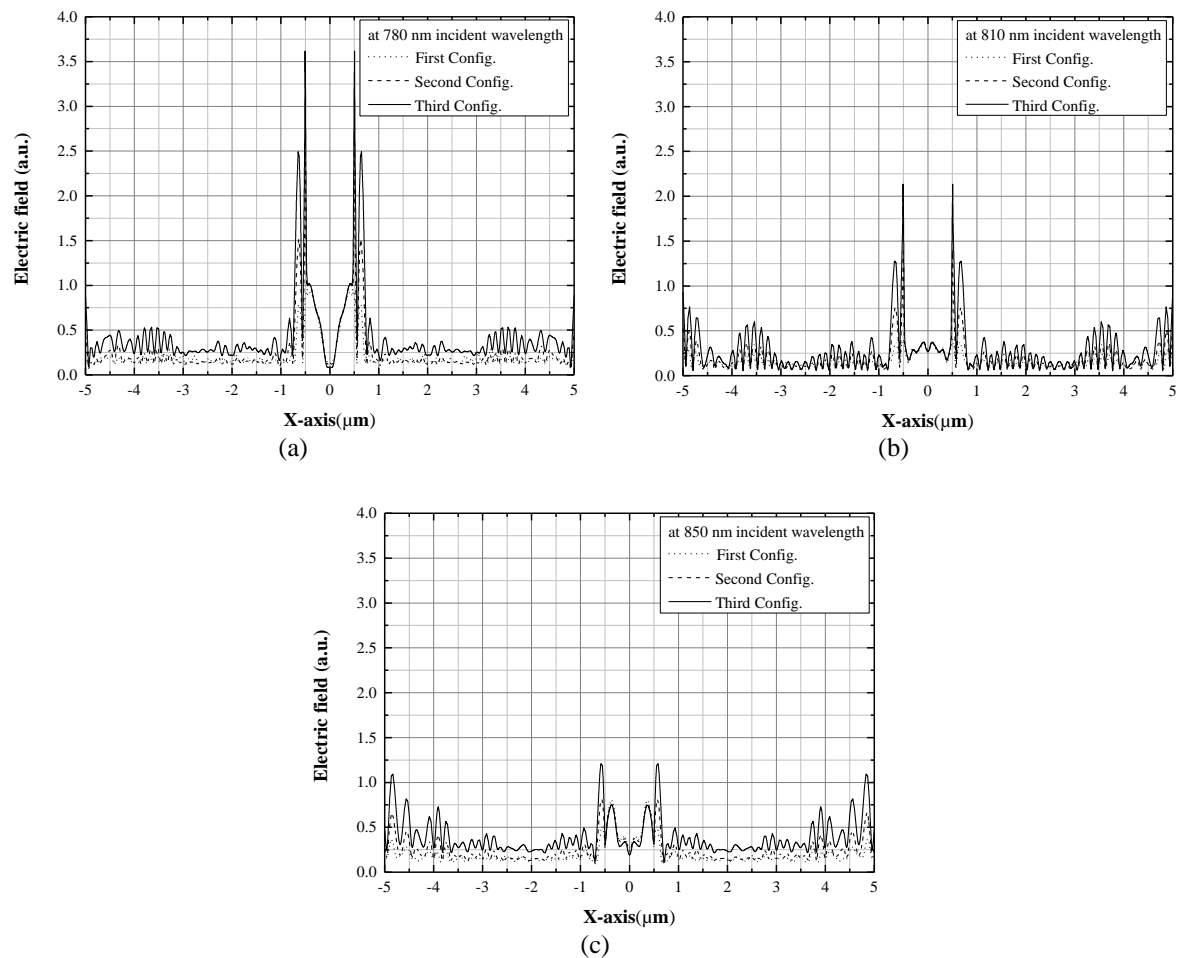


Figure 5. The electric field distributions along the structure x-axis on the surface of the Ag-NWs and in their gap region for the 1st, and the 2nd configurations and for the 3rd configuration with a GNA gap width of 124 nm at the following incident wavelengths: (a) 780 nm (b) 810 nm, and (c) 850 nm

The electric field distributions along the structure y-axis which crosses the center of Ag-NWs gap region are illustrated in Figures 6(a)-(c) for 780 nm, 810 nm, and 850 nm wavelengths, respectively. We have seen from Figures 3 and 5 that the third configuration with the smallest GNA gap width shows the highest electric field in comparison to the other configurations. In there, the small space between Ag-NWs and the GNA tip is responsible for increased light confinement near the nanowires. This high light confinement explains the highest enhancement for the third configuration with the smallest GNA gap width. Figure 7 illustrates the light confinement in the GNA gap region of 124 nm width near the Ag-NWs in the third configuration for the three incident wavelengths. The light confinement near the Ag-NWs is clearly showed by Figures 7(a)-(c) for 780 nm, 810 nm, and 850 nm wavelengths, respectively.

One of the factors that could affect the electric fields is the thickness of GNA and GND. Therefore, Figure 8 is presented to study the effect of changing the graphene thickness on the maximum electric fields for the three wavelengths. Three graphene thicknesses are selected. These are 7, 9, and 11 graphene layers

thicknesses. In the third configuration, the GNA gap width is fixed at 124 nm. The results show that the maximum electric field is inversely proportional to the graphene thickness. At 7 layers graphene thickness, the maximum electric field in the second configuration is (3.7, 2, and 4.2) times higher than the field in the first configuration for 780 nm, 810 nm, and 850 nm wavelengths, respectively. While, in the third configuration, the electric field is (4.1, 2.3, and 4.8) times higher for the aforementioned wavelengths, respectively.

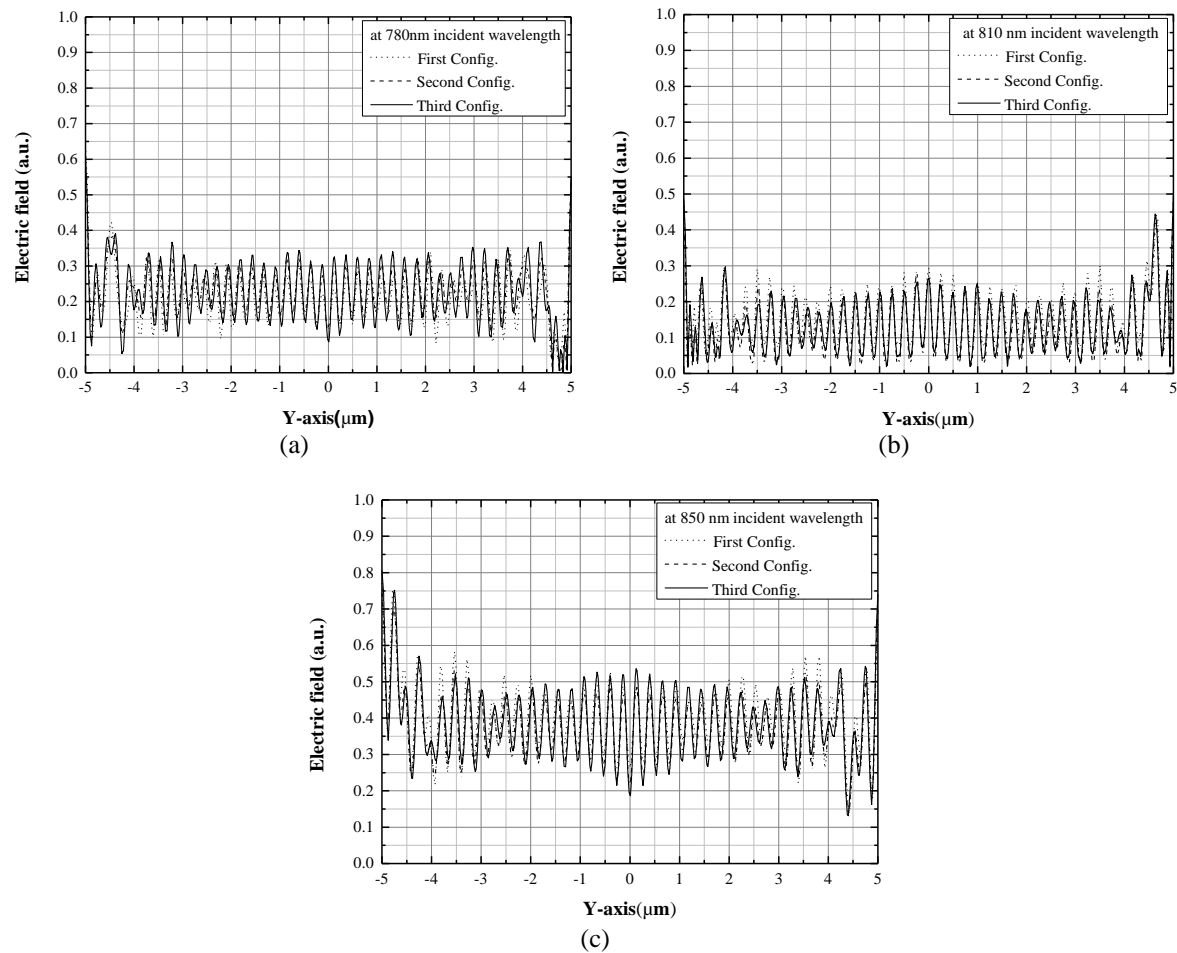


Figure 6. The electric field distributions along the structure y-axis which crosses the center of Ag-NWs gap region for the 1st, and the 2nd configurations and for the 3rd configuration with a GNA gap width of 124 nm at the following incident wavelengths: (a) 780 nm (b) 810 nm, and (c) 850 nm

From these results, we can conclude that the reduction in graphene thickness can also support the field enhancement in the hybrid configurations. By decreasing the thickness of GNA and GND to 7 layers of graphene, the maximum electric field in the photomixer is increased significantly. While at 11 layers thickness, the simulation results exhibit a very noticeable decline in the maximum electric field. The reason for this decline can be explained by the fact that the overlap between the conduction and the valance bands of graphene grows with the number of layers. Therefore, graphene above 10 layers is regarded as a thin film of graphite i.e., as a thin film of three-dimensional material [32]. Thus, the light confinement into graphene nano-dimensions would be reduced with increasing the thickness and cause a significant reduction in the electric field. When the graphene thickness is decreased to 7 layers thickness, the electric field is enhanced by 4.2 and 4.8 times in the second and third configurations, respectively. Moreover, the graphene thickness in the third configuration has a higher influence on the maximum electric field than in the second one, see Figure 8. The reason for this is that the small area of the GNA tip reinforces the light confinement and thus enhances the maximum electric field in the aforementioned configuration [33]. Therefore, the bow-tie shape of the GNA magnifies the effect of the graphene thickness on enhancing the electric field.

According to (1), the THz generated power is directly proportional to the square of the light intensity. Thus, the THz output power is proportional to the fourth power of the electric field. Therefore, the THz output power, at 850 nm excitation wavelength, can be enhanced by 310 and 530 times for the second and third configurations, respectively. Consequently, adding graphene as a nanoantenna array can enhance the conversion efficiency of the CW-THz photomixer in both configurations. By its unique properties, graphene can also contribute to improving the electrical and thermal conductivities in the device.

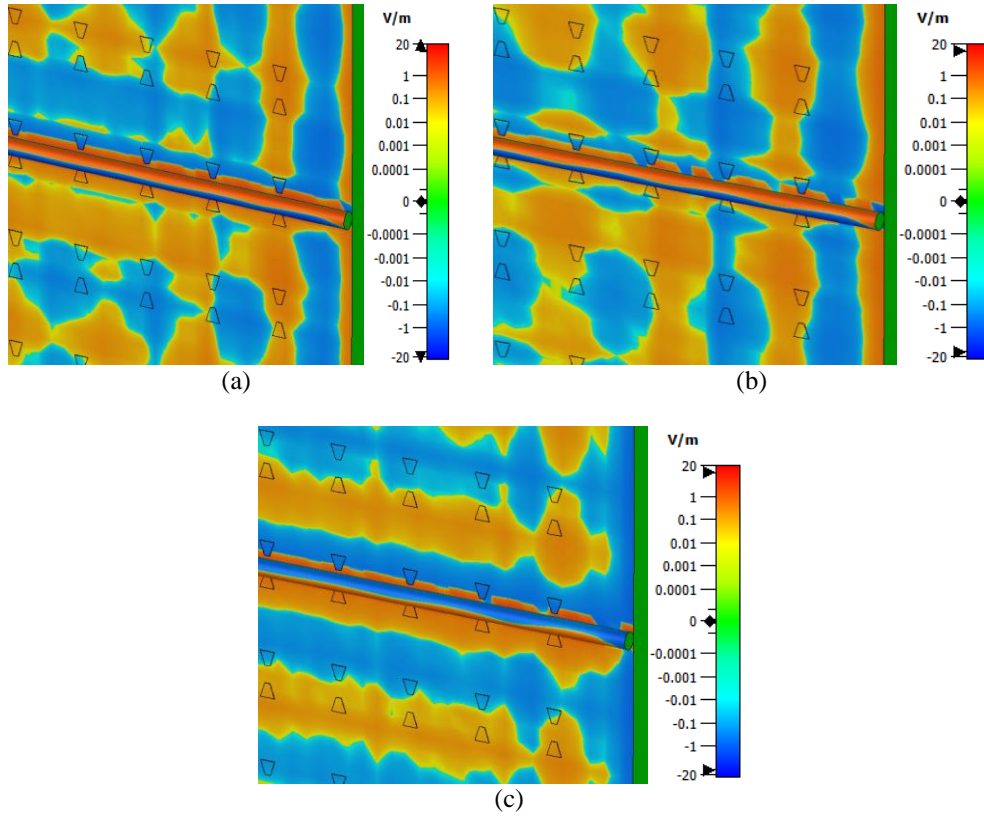


Figure 7. The distributions of the electric field z-component near Ag-NWs nanoelectrodes in the 3rd configuration with GNA gap width of 124 nm at the following incident wavelengths: (a) 780 nm, (b) 810 nm, and (c) 850 nm

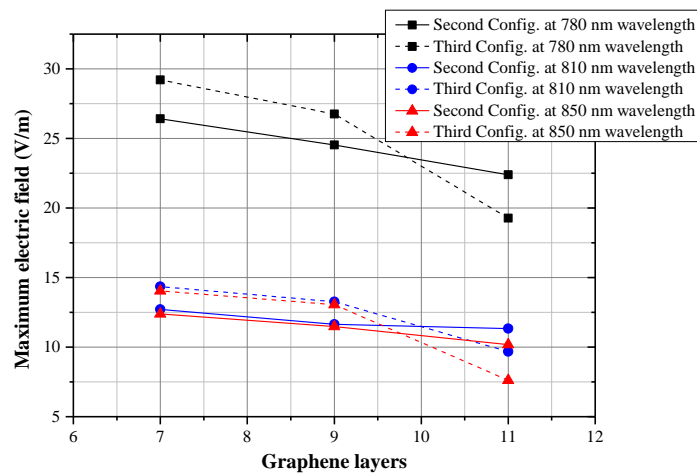


Figure 8. The maximum electric field in the 2nd and the 3rd configurations with GNA gap width of 124 nm versus graphene thickness for the three incident wavelengths

4. CONCLUSION

We have successfully proved that the electric field can be significantly enhanced in Ag-NWs based photomixer by adding graphene nanoantenna array as nanoelectrodes. In the two proposed photomixer configurations, the main enhancement comes from increasing the plasmonic effect of Ag-NWs. At 850 nm excitation wavelength, the THz output power can be enhanced by 310 and 530 times for GND and GNA array configurations, respectively. Moreover, by examining the simulation results, we have observed that the thickness of the graphene and the gap width of GNA play a crucial role in this enhancement. The effect of changing graphene chemical potential and Ag-NWs radii on the field enhancement will be considered as the future work for the two proposed configurations.




REFERENCES

- [1] R. Safian, G. Ghazi, and N. Mohammadian, "Review of photomixing continuous-wave terahertz systems and current application trends in terahertz domain," *Optical Engineering*, vol. 58, no. 11, Nov. 2019, doi: 10.1117/1.OE.58.11.110901.
- [2] A. A. A. Solyman and I. A. Elhady, "Potential key challenges for terahertz communication systems," *International Journal of Electrical and Computer Engineering (IJECE)*, vol. 11, no. 4, pp. 3403–3409, Aug. 2021, doi: 10.11591/ijece.v11i4.pp3403-3409.
- [3] B. St. Peter *et al.*, "Development and testing of a single frequency terahertz imaging system for breast cancer detection," *IEEE Transactions on Terahertz Science and Technology*, vol. 3, no. 4, pp. 374–386, Jul. 2013, doi: 10.1109/TTHZ.2013.2241429.
- [4] O. P. Cherkasova, M. M. Nazarov, M. Konnikova, and A. P. Shkurinov, "THz spectroscopy of bound water in glucose: direct measurements from crystalline to dissolved state," *Journal of Infrared, Millimeter, and Terahertz Waves*, vol. 41, no. 9, pp. 1057–1068, Sep. 2020, doi: 10.1007/s10762-020-00684-4.
- [5] S. Preu, G. H. Döhler, S. Malzer, L. J. Wang, and A. C. Gossard, "Tunable, continuous-wave terahertz photomixer sources and applications," *Journal of Applied Physics*, vol. 109, no. 6, Mar. 2011, doi: 10.1063/1.3552291.
- [6] D. J. Ironside, R. Salas, P.-Y. Chen, K. Q. Le, A. Alú, and S. R. Bank, "Enhancing THz generation in photomixers using a metamaterial approach," *Optics Express*, vol. 27, no. 7, pp. 9481–9494, Apr. 2019, doi: 10.1364/OE.27.009481.
- [7] E. R. Brown, "THz generation by photomixing in ultrafast photoconductors," *International Journal of High Speed Electronics and Systems*, vol. 13, no. 02, pp. 497–545, Jun. 2003, doi: 10.1142/S0129156403001818.
- [8] E. Pliński, "Terahertz photomixer," *Bulletin of the Polish Academy of Sciences: Technical Sciences*, vol. 58, no. 4, pp. 463–470, Jan. 2010, doi: 10.2478/v10175-010-0044-0.
- [9] M. Khabiri, M. Neshat, and S. Safavi-Naeini, "Hybrid computational simulation and study of continuous wave terahertz photomixers," *IEEE Transactions on Terahertz Science and Technology*, vol. 2, no. 6, pp. 605–616, Nov. 2012, doi: 10.1109/TTHZ.2012.2213596.
- [10] S. Matsuura and H. Ito, "Generation of CW terahertz radiation with photomixing," in *Terahertz Optoelectronics*, Berlin/Heidelberg: Springer-Verlag, 2005, pp. 157–202.
- [11] E. R. Brown, F. W. Smith, and K. A. McIntosh, "Coherent millimeter-wave generation by heterodyne conversion in low-temperature-grown GaAs photoconductors," *Journal of Applied Physics*, vol. 73, no. 3, pp. 1480–1484, Feb. 1993, doi: 10.1063/1.353222.
- [12] C. W. Berry, N. Wang, M. R. Hashemi, M. Unlu, and M. Jarrahi, "Significant performance enhancement in photoconductive terahertz optoelectronics by incorporating plasmonic contact electrodes," *Nature Communications*, vol. 4, no. 1, pp. 1622–1632, Jun. 2013, doi: 10.1038/ncomms2638.
- [13] C. W. Berry, M. R. Hashemi, S. Preu, H. Lu, A. C. Gossard, and M. Jarrahi, "High power terahertz generation using 1550 nm plasmonic photomixers," *Applied Physics Letters*, vol. 105, no. 1, Jul. 2014, doi: 10.1063/1.4890102.
- [14] C. W. Berry and M. Jarrahi, "Terahertz generation using plasmonic photoconductive gratings," *New Journal of Physics*, vol. 14, no. 10, Oct. 2012, doi: 10.1088/1367-2630/14/10/105029.
- [15] S.-H. Yang and M. Jarrahi, "Frequency-tunable continuous-wave terahertz sources based on GaAs plasmonic photomixers," *Applied Physics Letters*, vol. 107, no. 13, Sep. 2015, doi: 10.1063/1.4932114.
- [16] X. Li and S. K. Khamas, "Enhance the optical intensity of a THz photomixer using a plasmonic material filled two dimensional photonic crystal," in *Antennas and Propagation Conference 2019 (APC-2019)*, 2019, pp. 1–4, doi: 10.1049/cp.2019.0703.
- [17] R. M. Taha and H. A. Jawad, "Characterization of gold coating on nanostructured CR39 polymer as SERS sensor," *Iraqi Journal Laser*, vol. 17, no. A, pp. 17–22, 2018.
- [18] A. K. Ayal, "Enhanced photocurrent of titania nanotube photoelectrode decorated with CdS nanoparticles," *Baghdad Science Journal*, vol. 15, no. 1, pp. 57–62, 2018, doi: 10.21123/BSJ.15.1.57-62.
- [19] A. Hussein Duhis and M. Aljanabi, "Analysis and simulations of optimal geometry shapes of the 4 and 9 nano hole arrays (NHAs) with surface plasmonics and optical properties of biosensors systems," *International Journal of Electrical and Computer Engineering (IJECE)*, vol. 10, no. 3, pp. 2625–2632, Jun. 2020, doi: 10.11591/ijece.v10i3.pp2625-2632.
- [20] M. A. Gatea and H. A. Jawad, "Thermoplasmonic of single Au@SiO₂ and SiO₂@Au core shell nanoparticles in deionized water and poly-vinylpyrrolidone matrix," *Baghdad Science Journal*, vol. 16, no. 2, pp. 376–381, 2019, doi: 10.21123/bsj.2019.16.2.0376.
- [21] A. Mahmood, W. A. Jabbar, Y. Hashim, and H. Bin Manap, "Effects of downscaling channel dimensions on electrical characteristics of InAs-FinFET transistor," *International Journal of Electrical and Computer Engineering (IJECE)*, vol. 9, no. 4, pp. 2902–2909, Aug. 2019, doi: 10.11591/ijece.v9i4.pp2902-2909.
- [22] M. M. Wiecha *et al.*, "Direct near-field observation of surface plasmon polaritons on silver nanowires," *ACS Omega*, vol. 4, no. 26, pp. 21962–21966, Dec. 2019, doi: 10.1021/acsomega.9b03036.
- [23] S. Al-Daffaie *et al.*, "Silver nanowire surface plasmon polaritons enhancement in terahertz nanodevices," in *2019 44th International Conference on Infrared, Millimeter, and Terahertz Waves (IRMMW-THz)*, Sep. 2019, pp. 1–2, doi: 10.1109/IRMMW-THz.2019.8874523.
- [24] A. J. Jumaah, S. Al-Daffaie, O. Yilmazoglu, and T. Kusserow, "Continuous-wave terahertz emitter with hybrid nanoelectrodes based on graphene and nanowire," *OSA Continuum*, vol. 3, no. 7, pp. 1826–1833, Jul. 2020, doi: 10.1364/OSAC.392837.
- [25] I. Llatser, C. Kremers, A. Cabellos-Aparicio, J. M. Jornet, E. Alarcón, and D. N. Chigrin, "Graphene-based nano-patch antenna for terahertz radiation," *Photonics and Nanostructures - Fundamentals and Applications*, vol. 10, no. 4, pp. 353–358, Oct. 2012, doi: 10.1016/j.photonics.2012.05.011.




- [26] H. M. Marhoon and N. Qasem, "Simulation and optimization of tuneable microstrip patch antenna for fifth-generation applications based on graphene," *International Journal of Electrical and Computer Engineering (IJECE)*, vol. 10, no. 5, pp. 5546–5558, Oct. 2020, doi: 10.11591/ijece.v10i5.pp5546-5558.
- [27] M. Jabeen and S. Haxha, "High rear reflectance and light trapping in textured graphene based silicon thin film solar cells with back dielectric-metal reflectors," *OSA Continuum*, vol. 2, no. 5, pp. 1807–1821, May 2019, doi: 10.1364/OSAC.2.001807.
- [28] T. Stauber, N. M. R. Peres, and A. K. Geim, "Optical conductivity of graphene in the visible region of the spectrum," *Physical Review B*, vol. 78, no. 8, Aug. 2008, doi: 10.1103/PhysRevB.78.085432.
- [29] G. W. Hanson, "Dyadic Green's functions and guided surface waves for a surface conductivity model of graphene," *Journal of Applied Physics*, vol. 103, no. 6, Mar. 2008, doi: 10.1063/1.2891452.
- [30] Z. H. Ni *et al.*, "Graphene thickness determination using reflection and contrast spectroscopy," *Nano Letters*, vol. 7, no. 9, pp. 2758–2763, Sep. 2007, doi: 10.1021/nl071254m.
- [31] T. Hanke *et al.*, "Tailoring spatiotemporal light confinement in single plasmonic nanoantennas," *Nano Letters*, vol. 12, no. 2, pp. 992–996, Feb. 2012, doi: 10.1021/nl2041047.
- [32] B. Partoens and F. M. M. Peeters, "From graphene to graphite: electronic structure around the K point," *Physical Review B*, vol. 74, no. 7, p. 75404, Aug. 2006, doi: 10.1103/PhysRevB.74.075404.
- [33] M. I. Stockman, "Nanofocusing of optical energy in tapered plasmonic waveguides," *Physical Review Letters*, vol. 93, no. 13, Sep. 2004, doi: 10.1103/PhysRevLett.93.137404.

BIOGRAPHIES OF AUTHORS



Reiam Al-Mudhafar    received the B.Sc. and M.Sc. degrees in Laser and optoelectronics engineering from Al-Nahrain University, Baghdad, Iraq, in 2008 and 2014 respectively. Currently, she is Ph.D. student in Institute of Laser for Postgraduate Studies at the University of Baghdad. Her research interests include laser, THz technology, photonics, plasmonic, and optical communication. She can be contacted at email: reiam.al-mudhafar@ilps.uobaghdad.edu.iq.



Hussein Ali Jawad    received the B.Sc. degree in Physics from University of Mosul, Mosul, Iraq, in 1980 and the M.Sc. degree in laser from University of Baghdad, Baghdad, Iraq in 1993. He holds a PhD in Laser from University of Technology, Baghdad, Iraq, in 1999. Currently, he is the Dean of Institute of Laser for Postgraduate Studies at the University of Baghdad. His research interests include laser, nonlinear optics, photonics, and plasmonic. He can be contacted at email: hussein@ilps.uobaghdad.edu.iq.